23rd ABCM International Congress of Mechanical Engineering
December 6-11, 2015, Rio de Janeiro, RJ, Brazil

NUMERICAL INVESTIGATION OF THE NONLINEAR BEHAVIOR OF A DOUBLE PENDULUM

Guilherme Luiz Torres Mendonça [1]
Alberto Paiva [1]
Marcelo Amorim Savi [2]

[1] Universidade Federal Fluminense
Volta Redonda School of Engineering
Department of Mechanical Engineering
420 Trabalhadores Av.
Volta Redonda – RJ – Brazil – 27.255-250
guilhermeid@hotmail.com; paiva.ufrj@gmail.com (corresponding author)

[2] Universidade Federal do Rio de Janeiro
COPPE – Department of Mechanical Engineering
Center for Nonlinear Mechanics
Rio de Janeiro – RJ – Brazil – 21.941.972 – P.O. Box 68.503
savi@mecanica.ufrj.br

Abstract. *Elementary physical systems are often used to model practical mechanical applications; notwithstanding, despite of their simplicity, they may present complex nonlinear behaviors. In this regard, it is worthwhile to deeply understand their dynamical features, in order to explore all the richness of possible responses inherent to nonlinear systems, while dealing with real situations. This paper concerns the numerical analysis of a double pendulum, based upon topological interpretations. Differential equations of motion are implemented through a fourth-order Runge-Kutta scheme. Results accounts for a chaotic response associated to conservative behavior. Moreover, a discussion about toroidal bifurcation is also presented.*

Keywords: *Double pendulum, nonlinear dynamics, chaos, toroidal bifurcation.*

1. INTRODUCTION

Sometimes, the best solution is not associated with the most sophisticated. Simple mechanical systems can provide effective solutions of engineering problems with low cost. In this regard, consider the two following emblematic examples: Pesce et al. (1998) studied the launching dynamics and the anchoring of a catenary riser for the oil and gas industry, undergoing a simple pendulum motion; Battista and co-workers successfully designed synchronized vibration absorbers, by attaching discrete masses to strategic points of Rio-Niteroi bridge to avoid undesirable vibrations due to specific wind excitations (Hallak et al. 2013).

This general idea motivates the deep investigation of some classical dynamical problems, encouraging new applications related to these systems. Hence, even simple mechanical systems may present very complex behaviors, inasmuch they are taken in their nonlinear form. Therefore, it is imperative to thoroughly understand these irregular dynamical behaviors, such as chaos, before using them in practical applications.

The chaotic motion is a kind of response of nonlinear systems where its dimension should be, at least, three. Besides that, it is well-known that nonlinear systems are sensitive to slight changes in both initial conditions and system parameters, which drastically affect their response, which may easily vary from periodic to chaotic and vice-versa.

The study of nonlinear systems has evolved a lot in recently decades; however, much effort was devoted to low-dimensional dynamical systems that, nowadays, constitute a well-established subject in the literature. Concerning higher dimensional systems, some work has been done, concerning, for instance, spatiotemporal chaos (Umberger et al. 1989; Awrejcewicz, 1991; Shibata, 1998; Lai and Grebogi, 1999; Machado et al. 2003). In order to illustrate how higher dimensional systems may present more interesting phenomena, consider the fact that a typical one-degree of freedom system should be non-autonomous to present chaos, whereas systems with two or more degrees of freedom may present a chaotic response even for their natural behavior. In addition to that, these systems present some interesting topological aspects, due to their vector spaces with higher dimensions.

Within this scenario, double pendulum has been attracting the research community interest due to its complex dynamics and also to some technological applications. Grebogi, Yorke and co-authors performed a coupled numerical–experimental study of chaos in a double pendulum using *Lyapunov* exponents (Shinbrot et al. 1992). Lankalapalli & Ghosal (1996) modeled the dynamical movement of arms and legs as double pendula to study chaos in a robot control, while Cross (2005, 2011) employed the same approach to describe human sporting activities. Stachowiak & Okada (2006) and Tang et al. (2011) investigated the chaos occurrence in a double pendulum, while Szuminski (2014) studied the nonlinear dynamics (including chaos) of multiple pendula. Heyl (2008) and Small (2013) mapped the fractal structure presented by a double pendulum behavior, distinguishing rotating and non-rotating conditions.

This work deals with the dynamical investigation of the nonlinear behavior of a double pendulum. The resulting set of coupled ordinary differential equations is solved using a fourth-order Runge-Kutta scheme. Concerning the numerical results, firstly, the conservative behavior is examined, based upon topological interpretations. Trajectories in state subspaces, *Poincare* maps and bifurcation diagrams are obtained for different initial conditions, showing the route of the dynamical response from periodic towards chaotic behavior and the associated toroidal bifurcation. At last, *Lyapunov* exponents are analyzed to verify the nature of some of these results.

2. MATHEMATICAL MODELING

This section is dedicated to the dynamical formulation of the equations of motion for the double pendulum, using the Lagragean formalism. With this aim, consider the physical model presented in Fig. 1, where θ_1 and θ_2 are the absolute angular displacements of the internal and external pendula, respectively; L_1 and L_2 are the respective lengths of their rods; m_1 and m_2 are their respective masses; while $M_1(t)$ and $M_2(t)$ are the respective external excitation moments. The hypotheses adopted are: the rods are rigid and their masses are negligible compared to the bob masses m_1 and m_2; besides that, the system is submitted to gravitational body forces.

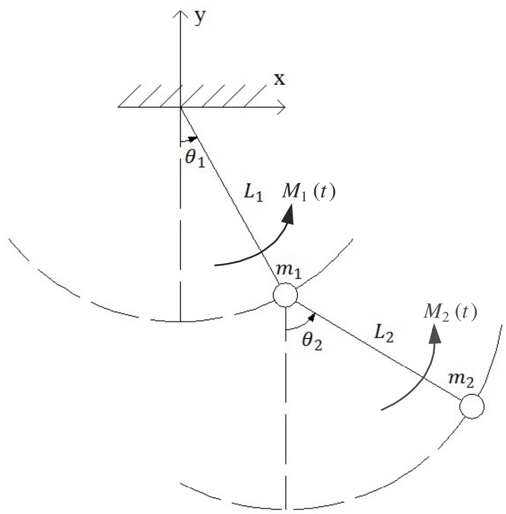

Figure 1. Physical model for the double pendulum.

Concerning the system kinematics, in order to obtain the energy expressions, consider the inertial reference frame of Fig. 1. It is possible to infer the vertical and horizontal displacements in "*x*" and "*y*" directions for masses m_1 and m_2, denoted by u_1, v_1, u_2 and v_2, respectively, which are derived to provide the associated velocities, according to Eq. (1).

$$\begin{aligned} u_1 &= L_1 \sin(\theta_1) & \dot{u}_1 &= L_1 \dot{\theta}_1 \cos(\theta_1) \\ v_1 &= -L_1 \cos(\theta_1) & \dot{v}_1 &= L_1 \dot{\theta}_1 \sin(\theta_1) \\ u_2 &= L_1 \sin(\theta_1) + L_2 \sin(\theta_2) & \dot{u}_2 &= L_1 \dot{\theta}_1 \cos(\theta_1) + L_2 \dot{\theta}_2 \cos(\theta_2) \\ v_2 &= -L_1 \cos(\theta_1) - L_2 \cos(\theta_2) & \dot{v}_2 &= L_1 \dot{\theta}_1 \sin(\theta_1) + L_2 \dot{\theta}_2 \sin(\theta_2) \end{aligned} \tag{1}$$

Euler-Lagrange's equation in its general form is given by Eq. (2), where: T is the total kinetic energy of the system; U is the total potential energy, while ϕ is the total dissipation energy. Besides, $\underline{q}$ is the generalized coordinates' vector; $\underline{Q}(t)$ is the generalized forcing vector; t is the independent variable time; whereas $(\dot{\ })$ corresponds to $(\dot{\ }) = d(\ )/dt$.

$$\frac{d}{dt}\left(\frac{\partial T}{\partial \underline{\dot{q}}}\right) - \frac{\partial T}{\partial \underline{q}} + \frac{\partial U}{\partial \underline{q}} = \underline{Q}(t) - \frac{\partial \phi}{\partial \underline{\dot{q}}} \qquad \text{where:} \quad \underline{q} = \begin{Bmatrix} \theta_1 \\ \theta_2 \end{Bmatrix} \tag{2}$$

The total kinetic energy (T) and the total potential energy (U) may be obtained by the summation ($T = T_1 + T_2$ and $U = U_1 + U_2$) of each of the two (internal and external) pendula, as follows:

$$\begin{aligned} T_1 &= m_1 \dot{\theta}_1^2 L_1^2 / 2 \quad \text{and} \quad T_2 = m_2 \left[\dot{\theta}_1^2 L_1^2 + \dot{\theta}_2^2 L_2^2 + 2 L_1 L_2 \dot{\theta}_1 \dot{\theta}_2 \cos(\theta_2 - \theta_1) \right] / 2 \\ U_1 &= -m_1 g L_1 \cos(\theta_1) \quad \text{and} \quad U_2 = -m_2 g \left[L_1 \cos(\theta_1) + L_2 \cos(\theta_2) \right] \end{aligned} \tag{3}$$

Similar consideration is adopted for the total dissipation energy (ϕ) given as follows, where C_1 and C_2 are the respective linear viscous damping coefficients.

$$\phi_1 = C_1 \, \dot{\theta}_1^2 \big/ 2 \qquad \text{and} \qquad \phi_2 = C_2 \, \dot{\theta}_2^2 \big/ 2 \tag{4}$$

Proceeding with the appropriate derivations assigned in Eq. (2) and considering harmonic excitations $M_1(t) = M_1 \cos(\Omega_1 t)$ and $M_2(t) = M_2 \cos(\Omega_2 t)$ acting on internal and external pendula, respectively, after some algebraic manipulation, the following equations of motion for the double pendulum arises:

$$\begin{aligned} &(m_1+m_2) L_1 \ddot{\theta}_1 + m_2 L_2 \cos(\theta_2-\theta_1)\ddot{\theta}_2 - m_2 L_2 \sin(\theta_2-\theta_1)\dot{\theta}_2^2 + C_1 \dot{\theta}_1 + (m_1+m_2)\, g \sin(\theta_1) = M_1 \cos(\Omega_1 t) \\ &m_2 L_1 \cos(\theta_2-\theta_1)\ddot{\theta}_1 + m_2 L_2 \ddot{\theta}_2 + m_2 L_1 \sin(\theta_2-\theta_1)\dot{\theta}_1^2 + C_2 \dot{\theta}_2 + m_2\, g \sin(\theta_2) = M_2 \cos(\Omega_2 t) \end{aligned} \tag{5}$$

where M_1 and M_2 are the forcing amplitudes imposed to the internal and external pendula, respectively, while Ω_1 and Ω_2 are their respective forcing angular frequencies.

For the purpose of numerical implementation via fourth-order Runge-Kutta, it is necessary to convert the original system consisting of two second-order ordinary differential equations into a new set of first-order ordinary differential equations with four equations. Hence, consider a variables' change, such that: $\theta_1 = x$; $\dot{\theta}_1 = y$; $\theta_2 = w$ and $\dot{\theta}_2 = z$.

$$\begin{cases} \dot{x} = y \\ \dot{y} = \dfrac{M_1 \cos(\Omega_1 t) - M_2 \cos(\Omega_2 t)\cos(w-x)}{L_1 \left[m_1 + m_2 \sin^2(w-x) \right]} - \dfrac{C_1\, y - C_2 \cos(w-x)\, z}{L_1 \left[m_1 + m_2 \sin^2(w-x) \right]} + \\ \quad + \dfrac{m_2 \sin(w-x) \left[L_1 \cos(w-x)\, y^2 + L_2\, z^2 \right]}{L_1 \left[m_1 + m_2 \sin^2(w-x) \right]} + \dfrac{g \left[m_2 \sin(2w-x) - (2m_1+m_2)\sin(x) \right]}{2 L_1 \left[m_1 + m_2 \sin^2(w-x) \right]} \\ \dot{w} = z \\ \dot{z} = \dfrac{-m_2 M_1 \cos(\Omega_1 t)\cos(w-x) + (m_1+m_2) M_2 \cos(\Omega_2 t)}{m_2 L_2 \left[m_1 + m_2 \sin^2(w-x) \right]} + \dfrac{m_2 C_1 \cos(w-x)\, y - (m_1+m_2) C_2\, z}{m_2 L_2 \left[m_1 + m_2 \sin^2(w-x) \right]} - \\ \quad - \dfrac{\sin(w-x) \left[(m_1+m_2) L_1\, y^2 + m_2 L_2 \cos(w-x)\, w^2 \right]}{L_2 \left[m_1 + m_2 \sin^2(w-x) \right]} - \dfrac{g\, (m_1+m_2) \left[\sin(w-2x) + \sin(w) \right]}{2 L_2 \left[m_1 + m_2 \sin^2(w-x) \right]} \end{cases} \tag{6}$$

3. NUMERICAL RESULTS

This section provides a numerical analysis of dynamical features concerning the double pendulum behavior. Initially, for a conservative system, the deformation of the toroidal phase space due to system sensitivity to initial conditions is evaluated through both trajectories evolution on state space and *Poincare* maps. Then, a discussion about the two natural mode shapes associated with the double pendulum is conducted, distinguishing periodic and quasi-periodic responses. Bifurcation diagrams varying the initial conditions allow the identification of some interesting phenomena, such as: the bifurcation of the toroidal phase space and the deconstruction of the toroidal structure under chaotic behavior. At last, *Lyapunov* exponents are evaluated to verify the different dynamical patterns previous obtained.

Before starting to present numerical results, some theoretical background should be provided, in order to better interpret the upcoming results. The double pendulum presents two independent *Degrees of Freedom* (**DOF**s), i.e. the absolute angular displacements θ_1 and θ_2 , each varying from 0 to 2π on each cycle, as shown in Fig. 2(a). If the circumference related to θ_1 is radially extruded along the θ_2 circumference, the resulting geometry is a torus, which characterizes the invariant manifold for the double pendulum. Consider a specific dynamical response evolving in the state space, confined within this torus. The trajectory described by this response strongly depends upon the two other state variables – the angular velocities $\dot{\theta}_1$ and $\dot{\theta}_2$ that, in turn, for a conservative system, have to do with the natural frequencies of the system. In this regard, it is possible to evaluate the ratio $d\theta_1 / d\theta_2 = \omega_1 / \omega_2$, where ω_1 and ω_2 are the natural frequencies, originating two different possibilities: if this ratio is rational (i.e. ω_1 and ω_2 are integers), a periodic trajectory with a closed orbit (known as trefoil knot) takes place; otherwise, a quasi-periodic trajectory appears instead. Figures 2(b) and 2(c), respectively, show these two behaviors. In Fig. 2(b), $\omega_1 = 3$ and $\omega_2 = 2$ are assumed.

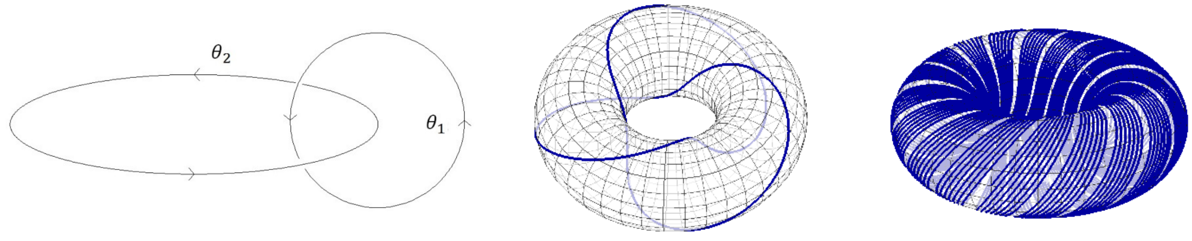

(a) (b) (c)

Figure 2. Toroidal phase space for the double pendulum. (a) Topological interaction of **DOF**s generating the torus; (b) Periodic trajectory upon torus surface; (c) Quasi-periodic trajectory upon torus surface.

In order to set parameters related to the natural behavior of the system to be used in the numerical simulations, the natural frequencies and natural modes are estimated from the eigenvalue-eigenvector problem associated with the linearized system of differential equations of motion (Eqs. 5), in its conservative form. Taking $m_1 = m_2 = m$ and $L_1 = L_2 = L$, the two vibration modes are given as follows, where $\underline{u}_1$ and $\underline{u}_2$ are the non-normalized natural modes.

$$\omega_1 = \sqrt{\frac{g}{L}}\sqrt{2-\sqrt{2}}\,; \quad \underline{u}_1 = \begin{Bmatrix} 1 \\ \sqrt{2} \end{Bmatrix} \qquad \text{and} \qquad \omega_2 = \sqrt{\frac{g}{L}}\sqrt{2+\sqrt{2}}\,; \quad \underline{u}_2 = \begin{Bmatrix} 1 \\ -\sqrt{2} \end{Bmatrix} \tag{7}$$

In the next simulations, all results refer to conservative behaviors. At this point, it is necessary to define a procedure to evaluate the *Poincare* sections. The adopted methodology focuses on the external pendulum analysis, which may be taken for a fixed reference position of the internal pendulum. Thus, the instantaneous values of the state variables associated with the external pendulum are stored, whenever the internal pendulum goes through the equilibrium position $\theta_1 = 0$, clockwisely.

In the first analysis, presented in Fig. 3, parameters are chosen in such a way to obtain quasi-periodic responses as follows: $m_1 = 3$ kg; $m_2 = 1$ kg; $L_1 = 2$ m; $L_2 = 1$ m and $g = 9.81$ m/s^2. Trajectories on state subspaces $\theta_1\times\theta_2\times\dot{\theta}_2$ and *Poincare* sections for state subspaces $\theta_2\times\dot{\theta}_2$ are displayed for three different initial conditions, considering only initial angular displacements with increasing values (with null initial angular velocities), according to Fig. 3 captions. In Fig. 3, the following initial conditions are adopted: for Figs. (a) and (d): $(\theta_{10}, \dot{\theta}_{10}, \theta_{20}, \dot{\theta}_{20}) = (10\pi/180; 0; 10\pi/180; 0)$; for Figs. (b) and (e): $(\theta_{10}, \dot{\theta}_{10}, \theta_{20}, \dot{\theta}_{20}) = (40\pi/180; 0; 40\pi/180; 0)$; for Figs. (c) and (f): $(\theta_{10}, \dot{\theta}_{10}, \theta_{20}, \dot{\theta}_{20}) = (80\pi/180; 0; 80\pi/180; 0)$. For all trajectories (Figs. 3a, 3b and 3c), there are no closed orbits, indicating quasi-periodic behaviors for all of them. *Poincare* sections in Figs. 3d and 3e present typical quasi-periodic responses, in agreement with their trajectories. While increasing the energy level of the system (greater initial angular displacement values), the toroidal structure is deformed and the respective *Poincare* sections become more complex, as the one obtained in Fig. 3(f).

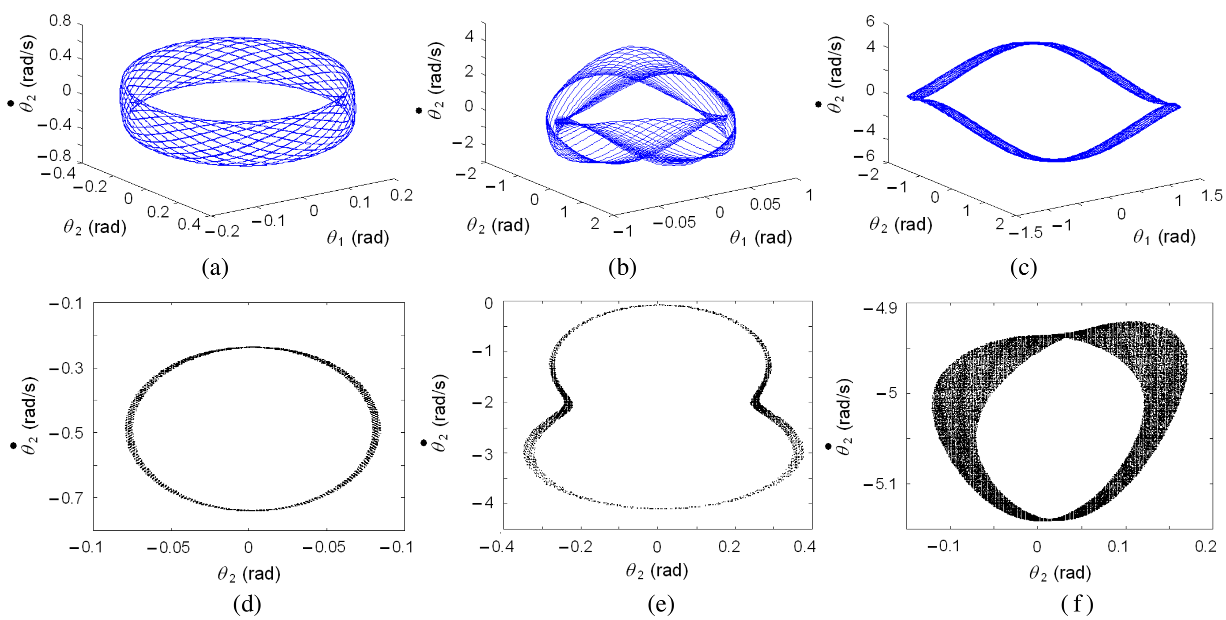

Figure 3. Dynamical analyses for different initial conditions. (a – c) State subspace; (d – f) Poincare section.

In the next simulations, present in Fig. 4, the target is to distinguish periodic from quasi-periodic responses by means of different energy levels (different initial conditions). This time, the parameters used respect the hypotheses set to obtain the vibration modes presented in Eq. (7); thus: $m_1 = m_2 = 1$ kg; $L_1 = L_2 = 1$ m and $g = 9.81$ m/s^2. In Figs. 4(a) and 4(b), the initial angular displacements are proportional to the first natural mode; while, in Figs. 4(c) and 4(d), they are proportional to the second natural mode. The difference between the cases 4(a) and 4(b) (as well as between 4c and 4d) is the magnitude of the angular displacement in each case – being a low energy level in cases 4(a) and 4(c) and a meaningful energy level in cases 4(b) and 4(d).

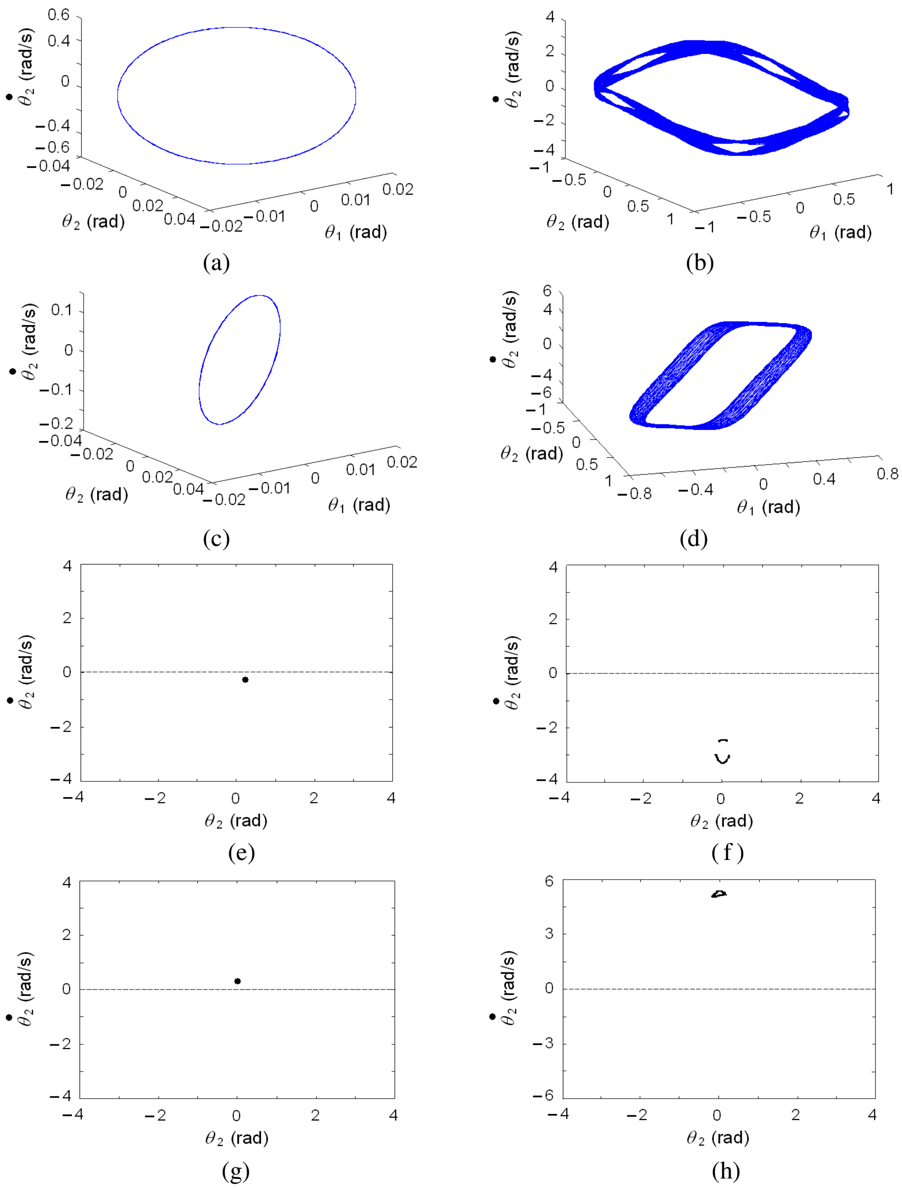

Figure 4. Dynamical analyses based on natural vibration modes presenting state subspace and Poincare sections.
(a – b) $(\theta_{10}, \dot\theta_{10}, \theta_{20}, \dot\theta_{20}) = (\pi/180; 0; \sqrt{2}\pi/180; 0)$; (c – d) $(\theta_{10}, \dot\theta_{10}, \theta_{20}, \dot\theta_{20}) = (40\pi/180; 0; 40\sqrt{2}\pi/180; 0)$;
(e – f) $(\theta_{10}, \dot\theta_{10}, \theta_{20}, \dot\theta_{20}) = (\pi/180; 0; -\sqrt{2}\pi/180; 0)$; (g – h) $(\theta_{10}, \dot\theta_{10}, \theta_{20}, \dot\theta_{20}) = (40\pi/180; 0; -40\sqrt{2}\pi/180; 0)$.

In Figs. 4(a) and 4(c), it is possible to identify periodic closed orbits related to the natural frequencies, as illustrated in Fig 2(a). The respective *Poincare* sections (Figs. 4e and 4g) present a single dot indicating a period-1 behavior for both of them. It is important to notice that in these two cases, the system behaves in the linear regime, due to the low energy level. In Figs. 4(b) and 4(d), quasi-periodic responses take place. They are associated with a higher energy level, which leads to a nonlinear regime. While reaching the nonlinear range, linear characteristics are dropped out and, despite of the fact that the initial conditions are proportional to each of the natural modes (inducing the same natural frequency in both pendula and, thus, turning the ratio ω_1/ω_2 unitary), the system behaves quasi-periodically.

Observing the *Poincare* sections of Fig. 4, it is possible to identify that, behaviors associated with the first natural mode (Figs. 4a and 4b), tend to occupy the inferior region (negative velocity $\dot{\theta}_2$) of the subspaces $\theta_2 \times \dot{\theta}_2$. On the contrary, behaviors related to the second natural mode (Figs. 4c and 4d) tend to occupy the superior region (positive velocity $\dot{\theta}_2$) of the same subspace. These observations can be justified based on the way the *Poincare* section is taken. For the first natural mode, both pendula oscillate in phase; therefore, when the internal pendulum goes through the equilibrium position $\theta_1 = 0$, clockwisely (negative velocity $\dot{\theta}_1$), the external pendulum has a negative velocity $\dot{\theta}_2$, as well. Analogously, for the second natural mode, the two pendula oscillate out of phase in opposite directions; as a result, when the internal pendulum goes through the equilibrium position $\theta_1 = 0$, clockwisely (negative velocity $\dot{\theta}_1$), the external pendulum has a positive velocity $\dot{\theta}_2$.

Figure 5 shows *Poincare* sections associated with quasi-periodic responses obtained for twenty different energy levels (different initial conditions), being ten related to the first mode and other ten to the second mode. This figure highlights the change in the map structure, while increasing the energy level.

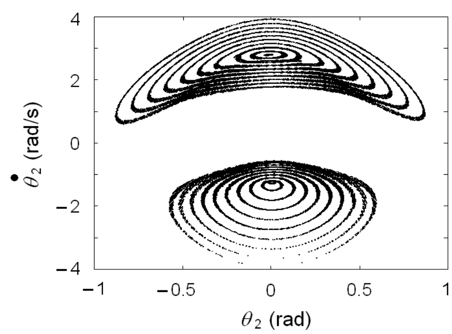

Figure 5. *Poincare* sections for state subspace $\theta_2 \times \dot{\theta}_2$ for different initial conditions.

The trajectory shown in Fig. 4(b) illustrates a particular phenomenon inherent to the double pendulum system – the toroidal bifurcation. Aiming a more detailed analysis of this feature, Fig. 6 presents a sequence of trajectories on the state subspace $\theta_1 \times \theta_2 \times \dot{\theta}_2$, considering different energy levels (initial conditions), varying from: $(\theta_{10}, \dot{\theta}_{10}, \theta_{20}, \dot{\theta}_{20}) = (30\pi/180; 0; 30\sqrt{2}\pi/180; 0)$ up to $(\theta_{10}, \dot{\theta}_{10}, \theta_{20}, \dot{\theta}_{20}) = (48\pi/180; 0; 48\sqrt{2}\pi/180; 0)$ with steps of 2π / 180 for θ_{10} and $2\sqrt{2}\pi/180$ for θ_{20}. According to this sequence, while the energy increases, a qualitative change in the toroidal structure is observed. It migrates from a quasi-periodic structure to a trajectory, which resembles a period-2 behavior (first figure in the second line). This change indicates that the ratio ω_1/ω_2 approaches a rational number. As the energy level remains increasing, the behavior reverts back into a quasi-periodic structure (suggesting that the ratio ω_1/ω_2 is deviating from a rational number); although, this time, in a bifurcated fashion, characterizing the toroidal bifurcation.

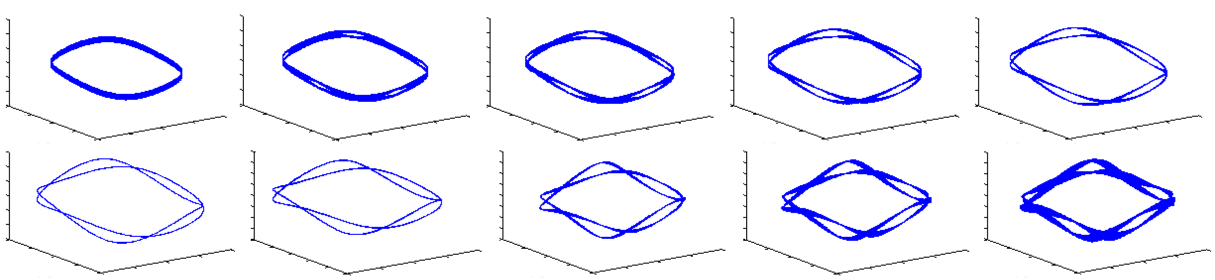

Figure 6. Qualitative change of the toroidal structure due to initial conditions variation.

As already observed in the previous results, for low energy levels, periodic and quasi-periodic responses take place. Besides, as the energy level increases, the toroidal structure is deformed. However, it may exist a trigger energy value from which the system suddenly becomes chaotic and the toroidal structure ends up completely deconstructed. Figures 7(a) and 7(b) show trajectories on state subspace $\theta_1 \times \theta_2 \times \dot{\theta}_2$ for two initial conditions very close one to another, according to Fig. 7 captions. The parameters used in this simulation are the same used for the ones in Fig. 4.

In Fig. 7(a), there is a well-defined quasi-periodic toroidal structure; whereas, in Fig. 7(b), there are tangled trajectories without a defined structure, suggesting a chaotic behavior. Figure 7(c) shows the *Poincare* section associated to the chaotic-like motion presented in Fig. 7(b). Since this behavior is obtained for a conservative situation, the presented structure may not be viewed as a strange attractor.

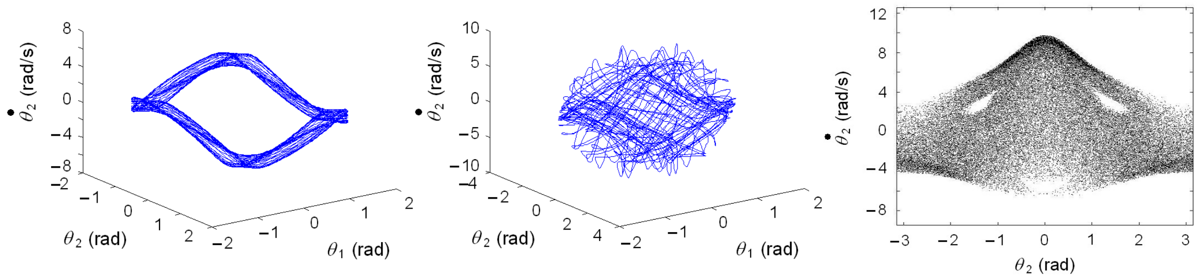

(a) (b) (c)

Figure 7. Deconstruction of the toroidal structure under chaotic behavior.

(a) Trajectory on state subspace $\theta_1 \times \theta_2 \times \dot{\theta}_2$ for $(\theta_{10}, \dot{\theta}_{10}, \theta_{20}, \dot{\theta}_{20}) = (79.1\pi/180; 0; 79.1\pi/180; 0)$;

(a) Trajectory on state subspace $\theta_1 \times \theta_2 \times \dot{\theta}_2$ for $(\theta_{10}, \dot{\theta}_{10}, \theta_{20}, \dot{\theta}_{20}) = (79.2\pi/180; 0; 79.2\pi/180; 0)$;

(c) *Poincare* section projection onto state subspace $\theta_2 \times \dot{\theta}_2$ for $(\theta_{10}, \dot{\theta}_{10}, \theta_{20}, \dot{\theta}_{20}) = (79.2\pi/180; 0; 79.2\pi/180; 0)$.

Figure 8 presents bifurcation diagrams varying simultaneously both initial conditions of angular displacements (θ_{10} and θ_{20}) for null initial angular velocities. Figures 8(a) and 8(b) show the route of the double pendulum behavior from periodic to chaotic motion. For very low values of initial conditions, a period-1 behavior takes place. As these values are increased, for moderate values, the behavior is quasi-periodic and, finally, for high values of initial conditions, a chaotic-like region occurs. It is worthwhile to notice that, since the adopted displacement initial conditions are all positive, the dynamical response for low energy levels are associated with the first (in phase) natural mode (with negative velocity $\dot{\theta}_2$), according to Fig. 8(a). The two values assigned in Fig. 8(c), which is a detailed projection of Fig. 8(b) in the plane $\theta_{20} \times \theta_2$, attest two past results. The first value $\theta_{20} \cong 0.98$ rad confirms the toroidal bifurcation identified in the first figure of the second line in Fig. 6, where the initial conditions are: $(\theta_{10}, \dot{\theta}_{10}, \theta_{20}, \dot{\theta}_{20}) = (40\pi/180; 0; 40\sqrt{2}\pi/180; 0)$. The second one $\theta_{20} \cong 1.38$ rad denotes the sudden transition from quasi-periodic to chaotic behavior assigned in Figs. 7(a) and 7(b). An interesting point is that this region around $\theta_{20} \cong 1.38$ rad, in the bifurcation diagram, corresponds to a cloud of points; however, it is not possible to distinguish the quasi-periodic behavior from the chaotic one.

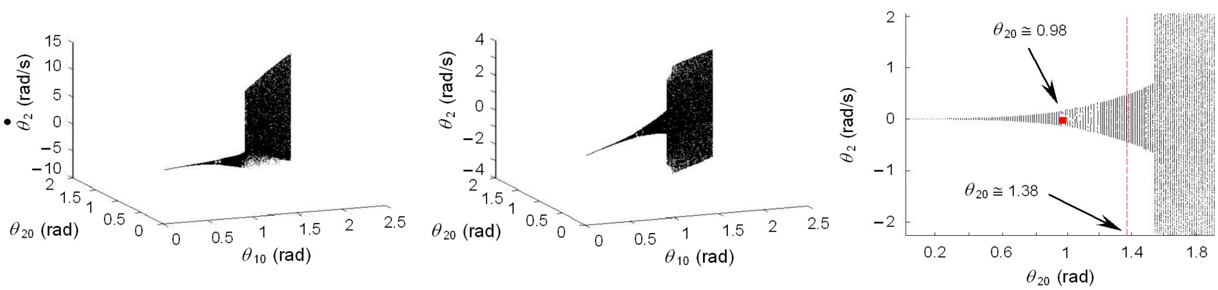

(a) (b) (c)

Figure 8. Bifurcation diagrams varying initial conditions. (a) θ_{10} x θ_{20} x $\dot{\theta}_2$; (b) $\theta_{10} \times \theta_{20} \times \theta_2$; (c) $\theta_{20} \times \theta_2$.

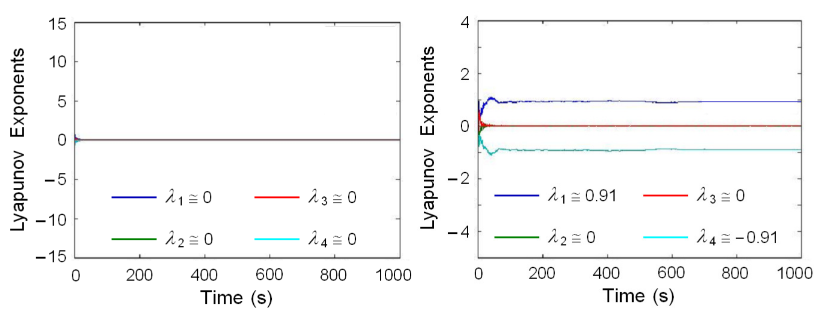

(a) (b)

Figure 9. Lyapunov spectra for different dynamical patterns.

(a) Quasi-periodic: $(\theta_{10}, \dot{\theta}_{10}, \theta_{20}, \dot{\theta}_{20}) = (79.1\pi/180; 0; 79.1\pi/180; 0)$;

(b) Chaotic: $(\theta_{10}, \dot{\theta}_{10}, \theta_{20}, \dot{\theta}_{20}) = (79.2\pi/180; 0; 79.2\pi/180; 0)$.

Figure 9 shows the *Lyapunov* spectra for two different dynamical patterns – periodic and chaotic behaviors, considering the two slight different initial conditions adopted in the simulation of Fig 7. In Fig. 9(a), all four exponents are null, which characterizes a periodic or quasi-periodic behavior (as a matter of fact, a quasi-periodic response, according to the trajectory on state subspace of Fig. 7a). In Fig. 9(b), two exponents are null, one is negative and the other is positive, confirming that, for $\theta_{10} = \theta_{20} \cong 1.38$ rad , the system is, in fact, chaotic. An interesting point that should be observed is that, in these two cases (Figs. 9a and 9b), as the system is conservative, the summation of all four exponents is null. This feature denotes that, in the case of Fig. 9(b), there may be directions of contraction and expansion but the volume of the system remains constant.

4. CONCLUDING REMARKS

This paper addresses the nonlinear analysis of a double pendulum. A thorough dynamical investigation is performed focused on its conservative behavior. Periodic and quasi-periodic motions are distinguished based upon topological interpretations, showing the toroidal deformation due to system sensitivity to initial conditions. Bifurcation diagrams varying the initial conditions help understanding the route of the double pendulum response from periodic to chaotic behavior. Besides, they attest the toroidal phase space bifurcation previously identified through trajectories in state subspaces. *Lyapunov* exponents are used to elucidate the difference between quasi-periodic and chaotic behavior, which was not clear in the bifurcation diagram.

5. ACKNOWLEDGEMENTS

The authors would like to acknowledge the support of the Brazilian Research Agencies CNPq, CAPES, FAPERJ as well as INCT-EIE (National Institute of Science and Technology - Smart Structures in Engineering). The acknowledgement applies also to Air Force Office of Scientific Research (AFOSR).

6. REFERENCES

Awrejcewicz, J.; 1991; “Bifurcation and Chaos in Coupled Oscillators”; *World Scientific Pub Co*; 250 pp.

Cross, R.; 2005; “A Double Pendulum Swing Experiment: in Search of a Better Bat”; *American Journal of Physics*; Vol.73; pp. 330–339.

Cross, R.; 2011; “A Double Pendulum Model of Tennis Strokes”; *American Journal of Physics*; Vol. 79; pp. 470–476.

Hallak, P.H. ; Pfeil, M.S.; Oliveira, S.R.C.; Battista, R.C.; Sampaio, P.A.B. & Bezerra, C.M.N.; 2013; “Aerodynamic Behavior Analysis of Rio-Niterói Bridge by means of Computational Fluid Dynamics”; “Engineering Structures” Vol. 56, pp. 935–944.

Heyl, J.S.; 2008; “The Double Pendulum Fractal”; *Department of Physics and Astronomy*; University of British Columbia, 8 pp.

Lai, Y.C. & Grebogi, C.; 1999; “Modeling of Coupled Chaotic Oscillators”. *Physical Review Letters*; Vol. 82; N. 24; pp. 4803–4806.

Machado, L.G.; Savi, M.A. & Pacheco, P.M.L.C.; 2003; “Nonlinear Dynamics and Chaos in Coupled Shape Memory Oscillators”; *International Journal of Solids and Structures*; Vol. 40; N. 19; pp. 5139–5156.

Pesce, C.P.; Aranha, J.A.P.; Martins, C.A.; Ricardo, O.G.S.; Silva S.; 1998; “Dynamics of Curvature in Catenary Risers at the Touch-down Point Region: an Experimental Study and the Analytical Boundary-Layer Solution”; *International Journal of Offshore and Polar Engineering*; Vol. 8; N. 3; pp. 302-310.

Rafat, M.Z.; Whealand, M.S. & Bedding, T.R.; 2009; “Dynamics of a Double Pendulum with Distributed Mass”; American Journal of Physics; Vol. 77; N. 3; 20 pp.

Shibata, H.; 1998; “Quantitative Characterization of Spatiotemporal Chaos”; *Physica A*; Vol. 252; pp. 428–449.

Shinbrot, T., Grebogi, C., Wisdom, J. & Yorke, J.A.; 1992; “Chaos in a Double Pendulum”; American Journal of Physics; Vol. 60; N.6; pp. 491–499.Lankalapalli, S. & Ghosal, A.; 1997; “Chaos in Robot Control Equations”; *International Journal of Bifurcation and Chaos*, Vol.7; pp. 707–720.

Small, A.; 2013; “Sample Final Project: One Signature of Chaos in the Double Pendulum”; *Department of Physics and Astronomy*, California State Polytechnic University, Pomona, CA.

Stachowiak, T. & Okada, T.; 2006; “A Numerical Analysis of Chaos in the Double Pendulum”; *Chaos, Solitons and Fractals*; Vol. 29, pp. 417–422.

Szuminski, W.; 2014; “Dynamics of Multiple Pendula Without Gravity”; *Chaotic Modeling and Simulation*; Vol. 1; pp. 57–67.

Tang, Y.; Groninger, E.; Foster, B.; Aliaga, D.; Buresh, T.R. & Madsen; M.J.; 2011; “Chaos of the Double Pendulum”; *Wabash Journal of Physics*; Vol. 2.3; pp.1–8.

Umberger, D.K.; Grebogi, C.; Ott, E. & Afeyan, B.; 1989; “Spatiotemporal Dynamics in a Dispersively Coupled Chain of Nonlinear Oscillators”; *Physical Review A*; Vol. 39; N. 9; pp. 4835–4842.

7. RESPONSIBILITY NOTICE